Fundamental understanding of goaf gas displacement in longwall goaf

K.M. Tanguturi[*] and R. Balusu

Energy Flagship, CSIRO, Pullenvale, Kenmore, Australia

Abstract

Fundamental understanding of the goaf gas distribution in a gassy coal mine is necessary for developing effective goaf gas drainage strategies in the longwall coal mine. The goaf gas was subjected to the surface and body forces that were classified depending upon whether they acted on the surface area or the volume of the gas element. Of these forces, the body forces were more predominant in displacing the goaf gas present in the underground mine. The buoyancy forces were classified as the body forces; they are the predominant forces acting on the goaf gas. The buoyancy forces depend mainly upon the density variation in the gas species and the panel orientation or panel geometry. If the temperature variations are neglected, the buoyancy forces that cause the displacement of the goaf gas depend mainly upon the panel orientation. In this work, numerical investigations were carried out using the computational fluid dynamics (CFD) techniques for the fundamental understanding of the goaf gas displacement for various panel orientations. The numerical results obtained for various panel orientations indicated that the goaf gas is displaced towards the tailgate (TG) side when the maingate (MG) was downdip, towards the MG side when MG was updip, towards the start-up of the panel when the face was downdip, and towards the face when the face was updip.

Keywords: *Maingate (MG), Tailgate (TG), Start-Up, Face, Panel.*

1. Introduction

Goaf gas emissions have increased substantially over the years, and are set to increase in a near future due to the high production rates, deep gassy mines, and trend in the industry towards wider and longer panels. In general, the goaf gas emission rates in a number of gassy mines are in the range of 500-6000 L/s. In addition to the high gas emission in the goaf area, the spontaneous coal combustion is also a major issue in many longwall panels. Therefore, it is important to have a fundamental understanding of the goaf gas distribution in the goaf for developing appropriate gas control and spontaneous combustion prevention strategies.

Numerical techniques such as the finite element and finite volume methods have been widely used from the past two decades for analyzing the gas and dust distribution in the underground longwall coal mines. Aziz et al. [1] have used these techniques to understand the ventilation mechanisms, and the gas and dust distributions in coal mines. Balusu et al. [2] have carried out numerical investigations to understand the goaf gas mechanism, and have proposed various inertisation strategies [3-5] for the prevention of spontaneous combustions in gassy coal mines. Balusu et al. [3] have also carried out numerical and field studies, and have investigated the gas drainage strategies in underground longwall mines. Ramakrishna Morla et al. [6-8] have investigated various optimization strategies for preventing sponcom in non-gassy coal mines, extracting coal by the blasting gallery method. Ren et al. [9] have investigated various inertisation options from the surface boreholes for sponcom prevention in the goaf. Krishna et al. [10-11] have investigated the gas distribution near the TG region for a gassy coal mine, and have suggested various options for controlling it. Roy et al. [15] have studied the gas management options for the reduced greenhouse gas emissions. Yarlagadda et al. [15] have numerically investigated the proactive inertisation strategies for the prevention of sponcom in non-gassy

blasting gallery panels. Although many papers exist, which discuss about the gas distributions and gas control strategies, the effect of panel orientations on the goaf gas distribution has not yet been presented in detail. It is always helpful to have a fundamental understanding of the goaf gas distribution, since such information would assist in developing the goaf gas drainage and proactive inertisation strategies. In this work, an attempt was made for the fundamental understanding of the goaf gas distribution varying the panel orientation.

The maingate (MG) orientation with respect to TG and face orientation has a critical effect on the goaf gas distribution in the goaf. The objective of this work was to have a fundamental understanding of the goaf gas distribution in the goaf for various panel orientations using the numerical techniques.

2. Geometry

The various dimensions used for developing the computational fluid dynamics (CFD) model are specified in Table 1. The length, width, and height of the model were 500, 300, and 95.6 m, respectively (Figure 1). The floor height was 12 m below the seam of 3.6 m thickness, and the goaf height was 80 m above the seam. Since the actual seam depth contours were not available for various combinations of the panel orientations, a simplified model was developed, and the orientation was incorporated in the CFD model (Figure 2).

Table 1. CFD model geometry dimensions.

Item/Descriptions	Full-scale
Length of goaf	500 m
Width of goaf	300 m
Goaf height above caving	80 m
Face width	10 m
Face height	3.6 m
Floor height below the face	12 m
Width of main/tail gate roadway	5.4 m

3. Modeling and meshing

The model was created in an ANSYS design modeler, and meshed using the default mesh tool (Figure 4). The total number of control volumes used for meshing the geometry was nearly 800,000, which lead to a mesh-independent solution. The dimensions of the cells in the face varied from 0.2 to 0.4 m, and the cell lengths varied from 0.5 to 2 m along the face. The cell

dimensions in the goaf region were very large, and varied between 2 m near the face and 10 m in the middle and at the panel start-up. The section-view of the face is shown in Figure 3.
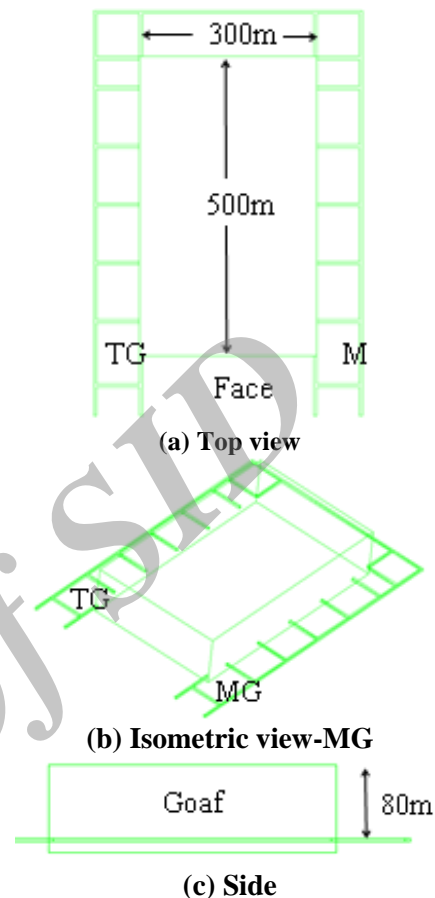

(a) Top view

(b) Isometric view-MG

(c) Side
Figure 1. Schematic representation of CFD model.

4. Mathematical models

The instantaneous conservative equation continuities, momentum, and species transport equations were solved numerically using the finite volume discretisation techniques [12]. These equations were solved in the laminar flow goaf region, which was treated as the porous medium region with resistances varying in all the three directions. The front leg, lemniscate linkages, and canopy of the chucks, which were in the face, were modeled as the porous zones. The porous media model in the FLUENT solver was used to simulate the flow though these regions by the introduction of a source term to the standard fluid flow equations. The source term was composed of two parts: a viscous loss term (Darcy law), and an inertial loss term.

4.1. Instantaneous equations

Continuity equation:

$$\nabla \bullet \vec{V} = 0.0 \tag{1}$$

Steady state Navier-Stokes equation:

$$(\vec{V} \bullet \nabla)\rho \vec{V} = -\nabla p + \mu \nabla^2 \vec{V} + \rho \vec{f} + \vec{S} \qquad (2)$$

Steady state species transport equation:

$$(\vec{V_s} \bullet \nabla)\rho Y_s = D_{m_s}\nabla^2 Y + \dot{\omega_s} \qquad (3)$$

where the subscript s represents the properties of O_2, CH_4, and N_2.

$$\vec{S} = -\left(\sum_{j=1}^{3} D_{ij}\mu\vec{V} + \sum_{j=1}^{3} C_{ij}\frac{1}{2}\rho|\vec{V}|\vec{V} \right) \qquad (4)$$

The source term in the momentum equation

contributes to the pressure gradient in the porous cell, which is proportional to the fluid velocity in the cell. Further information regarding the model can be obtained in the ANSYS FLUENT manual [13]. In the CFD model, the incorporation of the goaf spatial permeability distribution and the gas emission rates were via the user defined function (UDF), which was linked to the FLUENT solver.
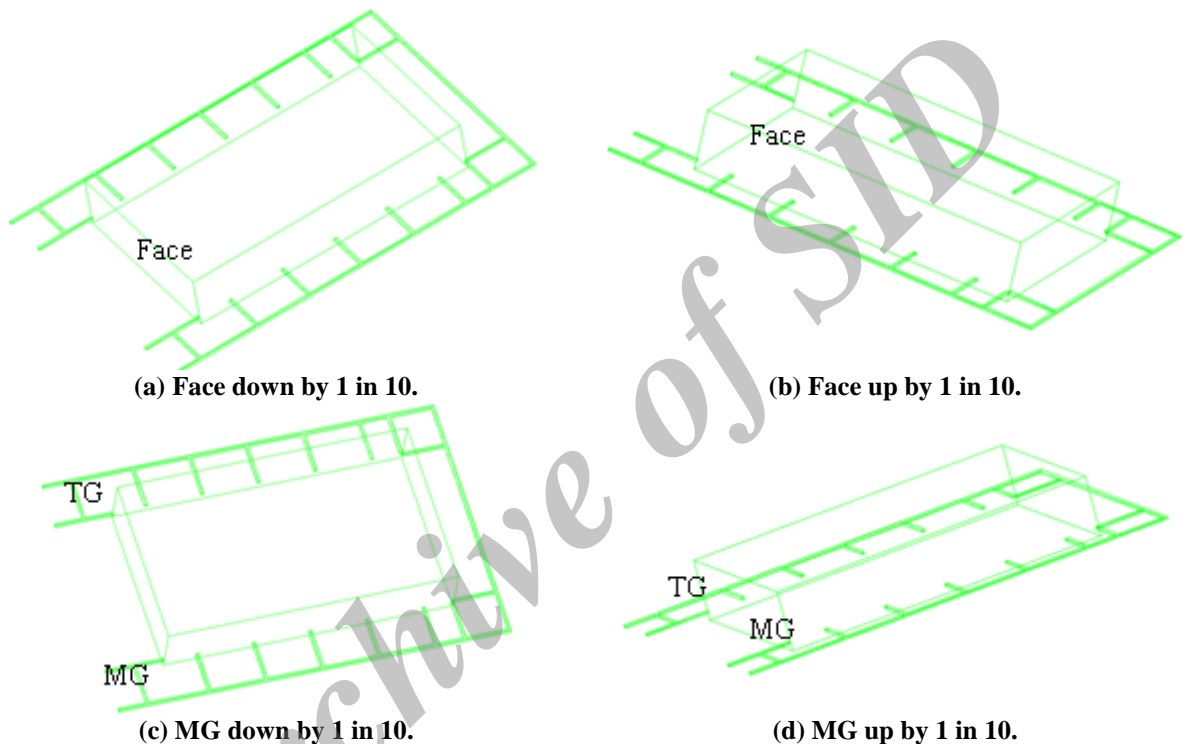

(a) Face down by 1 in 10.

(b) Face up by 1 in 10.

(c) MG down by 1 in 10.

(d) MG up by 1 in 10.

Figure 2. Schematic representation of CFD model with different panel orientations.
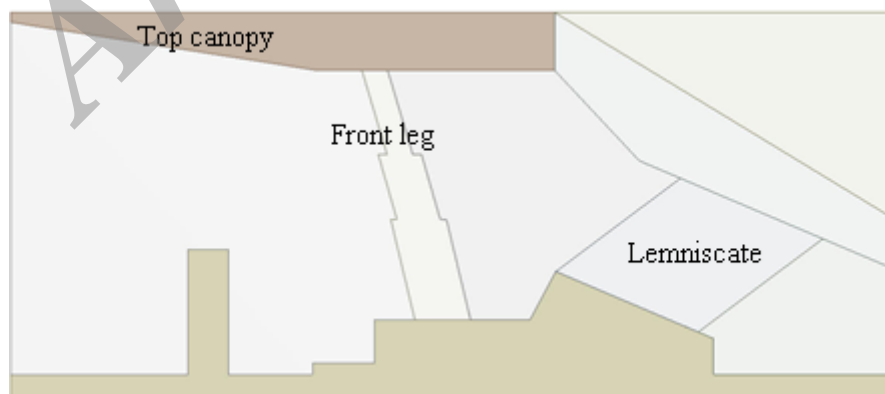

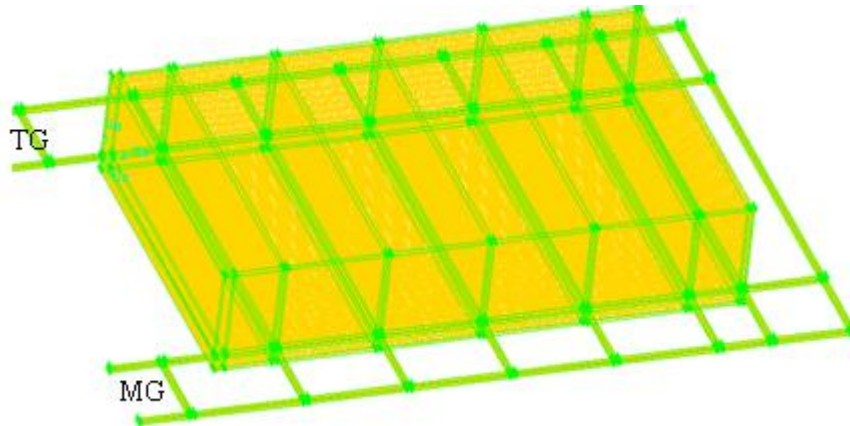**Figure 3. Schematic representation of cross-section of the face.**

193

Figure 4. Meshed model.

4.2. Time-averaged governing equations

In the face region, the flow was treated as the turbulent, and the time/Reynolds-averaged equations were solved. The two-equation standard k-epsilon model [14] was used to determine the eddy viscosity and the Reynolds stress tensor.
Time-averaged continuity equation:

$$\nabla \bullet \vec{V} = 0.0 \tag{5}$$

Reynolds-averaged Navier-Stokes equation:

$$(\vec{V} \bullet \nabla)\rho\vec{V} = -\nabla\overline{P} + \mu\nabla^2\vec{V} + \nabla : \tau_R \tag{6}$$

where τ_R is the Reynolds stress tensor.
Turbulent kinetic energy-k equation:

$$\rho\overline{u_j}\frac{\partial k}{\partial x_j} = \tau_{ij}\frac{\partial \overline{u_i}}{\partial x_j} + \frac{\partial}{\partial x_j}\left((\mu + \frac{\mu_T}{\sigma_k})\frac{\partial k}{\partial x_j}\right) - \rho\varepsilon \tag{7}$$

where the subscript j represents the Einstein summation notation.
Turbulent dissipation-ε equation:

$$\rho\overline{u_j}\frac{\partial \varepsilon}{\partial x_j} = C_{\mu1}\tau_{ij}\frac{\partial \overline{u_i}}{\partial x_j} +$$
$$\frac{\partial}{\partial x_j}\left((\mu + \frac{\mu_T}{\sigma_\varepsilon})\frac{\partial \varepsilon}{\partial x_j}\right) - C_{\mu2}\rho\frac{\varepsilon}{k^2} \tag{8}$$

where Cμ1 and Cμ2 are the closure coefficients.
Reynolds stress:

$$\tau_{ij} = \mu_T\left(\frac{\partial \overline{u_i}}{\partial x_j} + \frac{\partial \overline{u_j}}{\partial x_i}\right) - \frac{2}{3}\rho k \delta_{ij} \tag{9}$$

where μ_T is the eddy viscosity, and δ_{ij} is the Kronecker delta.
Eddy Viscosity:

$$\mu_T = c_\mu \rho \frac{k^2}{\varepsilon} \tag{10}$$

where c_μ is the closure coefficient, which is equal to 0.07.

The first order schemes were used to discretize the governing equations, as the cell size was very large in the goaf and the second order schemes failed to converge. Coupling between the pressure term and velocity was implemented using the SIMPLE algorithm, developed by Patankar [12]. In the goaf region, the air flow was assumed to be laminar, and the instantaneous equations were solved. In the face, the flow was turbulent, and the time-averaged steady state equations were solved here. The standard κ-ε model was used to calculate the additional stresses induced in the flow due to turbulence. All the governing equations were solved until the convergence criterion of the order 10^{-5} was reached.

4.3. Boundary conditions

At the MG inlet, an inlet velocity of 2.05 m/s corresponding to the flow rate of 40 m³/s across the face was specified, and at the TG outlet, the outflow boundary condition was specified. The buoyancy effects were incorporated in the model via the gravity components along the x and z directions, which is a function of the goaf orientation. The gravity was resolved along the x and z directions based on the panel orientation. In the goaf, a CH_4 gas emission rate of 500 L/s was specified via UDF as the source term to the species transport equation.

5. Validations

The results obtained numerically were compared with the measured field data for the validation of the results. Figures 5 and 6 show the comparison between the field data and the simulated velocities at the mid-face and at 5 m from the TG corner. Figure 5a show the field data measured at various locations across the mid-face using an

194

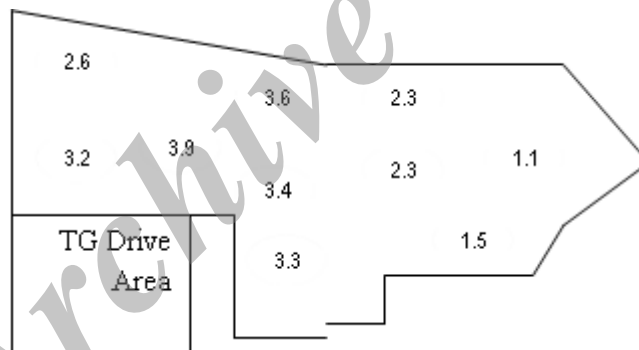anemometer, which was in concurrent with the   simulated results.
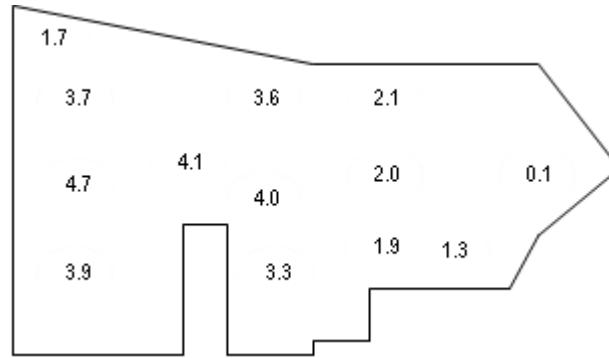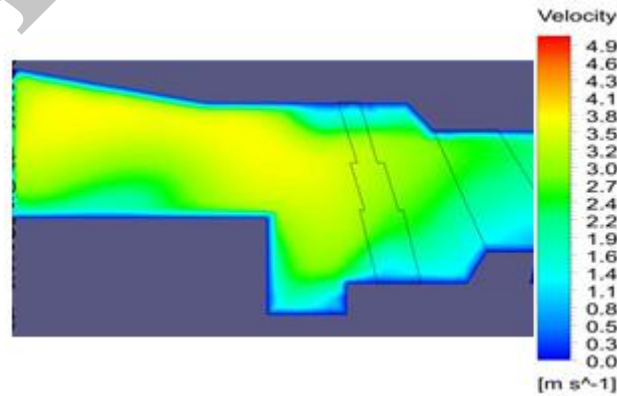

(a) Velocity field data at mid-face in m/s.
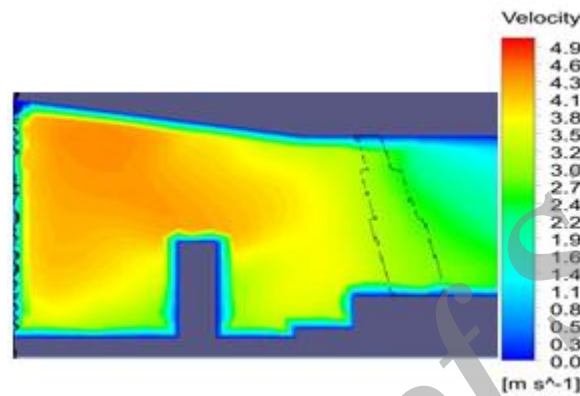
(b) Simulated velocities at mid-face.
Figure 5. Measured and simulated velocities at mid-face.

(a) Velocity field data in m/s at 5 m from TG

(b) Simulated velocities at 5 m from tailgate.
Figure 6. Measured and simulated velocities at TG.

195

At the mid-face, the flow was fully developed, and high velocities were observed near the face. The velocities reduced across the face till the back of the face due to the flow restrictions from the front leg, lemniscate linkages, and canopy, which were treated as porous media in the model. Figure 6a indicates the field data at various locations across the face before 5 m from the TG exit. In Figure 6b, at 5 m before the TG exit, the simulated velocities in the face were in concurrent with the measured field data, and it was concluded that the simulation results were reliable for further parametric studies.

6. Results and discussion

Numerical simulations were carried for the flat gradient of the face, i.e. with no elevation difference between the MG and TG sides of the panel. Figure 7a shows the methane gas distribution in the plane, which is 2 m above the floor, containing the face. The methane gas is more or less distributed symmetrically in the goaf with a gas concentration of 75% at the centre and varying between 5 and 20% on the MG side of the goaf. At the start-up of the panel, the methane gas concentrations varied between 45 and 60%. Since the methane gas is less dense compared to the nitrogen and oxygen species, it settled in the upper regions of the goaf. Figures 7b and 7c show the methane gas distribution in the plane at 50 and 70 m above the face. The methane gas distribution was symmetric, and a high concentration of 80% was observed at the centre of the goaf. At 50 m above the face (Figure 7b), the methane gas concentration was around 30% behind the face, and it was 65% in the start-up area. At 70 m above the face (Figure 7c), the methane gas concentration increased further to 55 and 80% behind the face and in the start-up area.

Figure 8 shows the methane gas distribution in the goaf at various locations for the panel with MG downdip. As shown in Figure 8a, the methane gas distribution in the plain containing the face was not more symmetric, and the gas was pulled more towards the TG side of the goaf due to the buoyancy effects on the lighter methane gas. At the start-up area of the panel, the methane gas concentration varied between 15 and 25%, and behind the face, it was below 5%. The methane gas concentration on the MG side of the goaf was below 5%, and on the TG side, it was below 30%. Figures 8b and 8c show the methane gas distribution in the plane at 50 and 70 m above the face. The methane gas distribution was non-

symmetric, and a high concentration of it (above 80%) was observed in the mid-length of the panel on the TG side. Behind the face and at the start-up area, the methane gas concentration reached around 30% at 50 m above the face, and increased to 40-45% at 70 m above the face.

Figure 9 shows the methane gas distribution in the goaf at various locations for the panel with MG updip. As shown in Figure 9a, the methane distribution was non-symmetric, and the gas was pulled more towards the MG side of the goaf. At the start-up area of the panel, the methane gas concentration was between 10 and 15%, and behind the face, its concentration was below 5%. On the MG side of the goaf, it increased compared to the case with MG downdip. The methane gas concentration varied between 5 and 30% on the MG side, and it was below 5% on the TG side and in the TG cut-through region. The methane gas was confined at the mid-length on the MG side of the panel, as shown in Figures 9b and 9c. A high methane gas concentration (above 80%) was observed at the mid-length of the panel on the MG side. Behind the face and at the start-up area, the methane gas concentration reached around 30% at 50 m above the face, and increased to 40-60% at 70 m above the face.

Figure 10 shows the methane gas distribution for the panel with the face downdip. As shown in Figure 10a, the methane gas distribution was symmetric, and the gas was pulled towards the start-up area of the panel. In this area, the methane gas concentration was high (up to 75%), and behind the face, it was below 5%. On the MG and TG sides and in the cut-through region of the goaf, the methane gas concentration varied between 5 and 65%. As shown in Figures 10b and 10c, the methane gas was confined from the mid-length of the goaf to the start-up area of the panel in the upper region of the goaf above 50 and 70 m. The methane gas distribution was non-symmetric, and a high concentration of it (above 80%) was observed in the mid-length and in the start-up area above 50 and 70 m of the face. Behind the face and at the start-up area, the methane gas concentration was around 30 and 75% at 50 m above the face, and it increased to 60 and 80% at 70 m above the face.

Figure 11 shows the methane gas distribution for the panel orientation with the face updip. As shown in Figure 11a, the methane gas was symmetric, and the gas was pulled behind the face of the panel. At the start-up area, the methane gas

concentration was 15%, and behind the face, it was below 5%. On the MG side and in the cut-through region, the methane gas concentration was below 5%. The methane gas settled at the centre of the goaf, as shown in Figures 11b and 11c. The methane gas distribution was symmetric, and a high concentration of it (above 80%) was observed near the mid-length of the panel. Behind the face and near the start-up area, the methane gas concentration was around 30% at 50 m above the face, and it increased to 75 and 30% at 70 m above the face. A high concentration of it was observed above the face when the face oriented updip.

The outcomes of the numerical simulations with various panel orientations were presented in a tabular form (Table 2). Based on these results, the mine designs could be interpreted for developing effective goaf gas drainage strategies.

For the flat panel, the goaf gas would settle in the centre of the goaf and in the start-up area of the panel. For the high goaf gas drainage, the goaf holes on the TG side, MG side, and near the start-up area of the panel were recommended. For the prevention of sponcom, inertisation on the MG side of the panel would be recommended. Since the methane gas diffuses near the start-up area of the panel, the oxygen levels were diluted; the chance of sponcom would be negligible. Inertisation near the start-up area of the panel would be optional.

For the panel with MG downdip, the goaf gas would settle on the TG side of the goaf. For a high goaf gas drainage, the goaf holes on the TG side were recommended. Performance of the goaf holes on the MG side of the goaf would be very less. Since the methane concentration on the MG side and in the start-up area was low, more oxygen levels and a greater chance of sponcom in the goaf were expected. For the prevention of sponcom, inertisation on the MG side and near the start-up area of the panel would be recommended.

For the panel with MG updip, the goaf gas would settle on the MG side of the goaf. For a high goaf gas drainage, the goaf holes on the MG side were recommended. Performance of the goaf holes on the MG side of the goaf would be high compared

to the TG side of the goaf holes. Since the methane concentration in the start-up area was low, more oxygen levels and a greater chance of sponcom in the goaf were expected. For the prevention of sponcom, inertisation near the start-up area of the panel would be recommended.

For the panel with the face downdip, the goaf gas was widely distributed in either side of the goaf and near the start-up area of the panel. For a high goaf gas drainage, the goaf holes on the TG side, MG side, and near the start-up area of the panel were recommended. Since the methane concentration in the start-up area was very high, less oxygen levels were expected, and the chance of sponcom in the start-up area of the panel was negligible. For the prevention of sponcom, inertisation behind the face of the panel would be recommended.

For the panel with the face updip, the goaf gas was widely distributed in the goaf. For a high goaf gas drainage, the goaf holes on the TG and MG sides were recommended. Since the methane concentration in the start-up area was very low, high oxygen levels were expected, and the chance of sponcom in the start-up area of the panel was high. For the prevention of sponcom, inertisation behind the face of the panel and in its start-up area would be recommended.

7. Conclusions

From the numerical simulations carried out, it was concluded that the goaf gas distribution depended on the panel orientation, and the methane gas concentration varied with the orientation of the panel. The methane gas settled on the MG side of the goaf when the MG was updip, on the TG side of the goaf when the MG was downdip, near the start-up area when the face was downdip, and, finally, near the face when the face was updip. It was concluded that the fundamental understanding of the goaf gas distribution would be helpful in determining the goaf gas drainage strategies and inertisation options in the goaf.

Table 2. Outcomes of numerical simulations in plane containing the face.

Panel orientation	Gas settlement	CH$_4$% MG side	CH$_4$% TG side	CH$_4$% Behind face	CH$_4$% Startup
Flat	Centre of goaf	5-20	5-65	0-5	45-60
MG downdip	TG side of goaf	0-5	0-30	0-5	15-25
MG updip	MG side of goaf	5-30	0-5	0-5	10-15
Face downdip	Start-up of panel	5-65	5-65	0-5	70-75

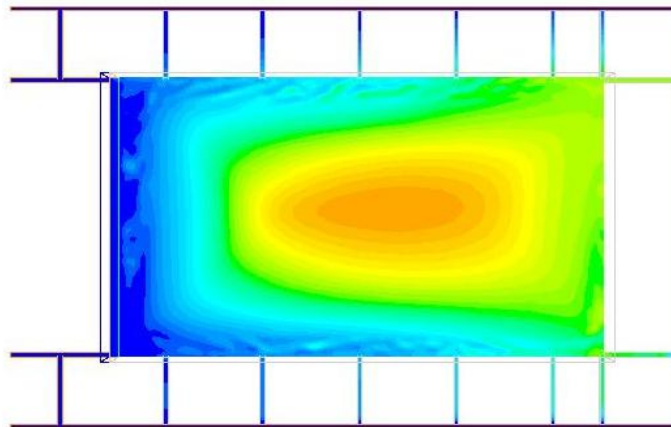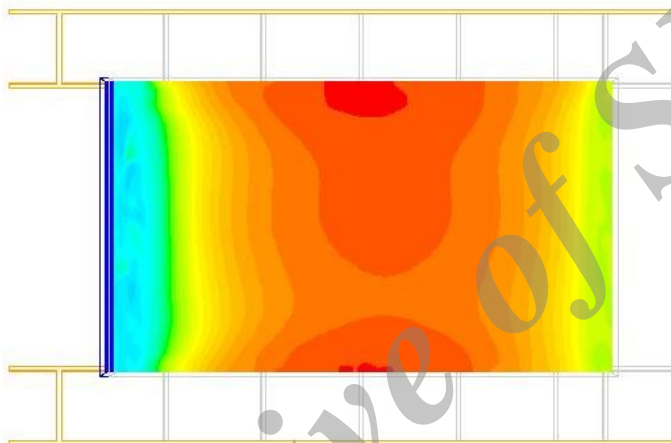| Face updip	Behind face	0-5	5-30	0-5	5-15

(a) Gas distribution in plane containing the face.

(b) Gas distribution in plane 50 m above the face.

(c) Gas distribution in plane 70 m above the face.

Figure 7. Goaf gas distribution for flat panel

198

(a) Gas distribution in plane containing the face.

CH₄ Conc.

1.00
0.95
0.90
0.85
0.80
0.75
0.70
0.65
0.60
0.55
0.50
0.45
0.40
0.35
0.30
0.25
0.20
0.15
0.10
0.05
0.00

(b) Gas distribution in plane 50 m above the face.

(c) Gas distribution in plane 70 m above the face.

Figure 8. Goaf gas distribution for panel with MG downdip.
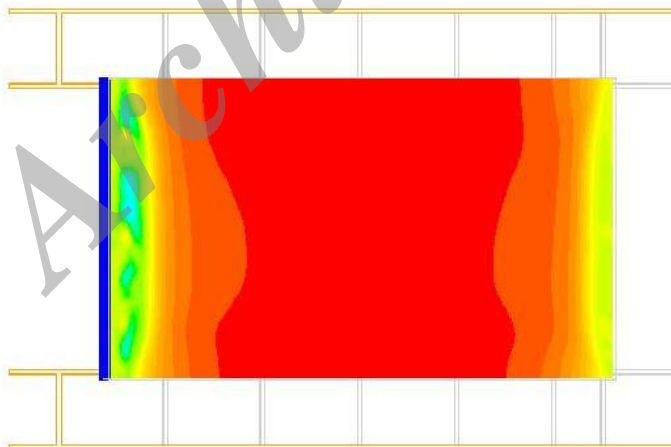
199

(a) Gas distribution in plane containing the face.

(b) Gas distribution in plane 50 m above the face.
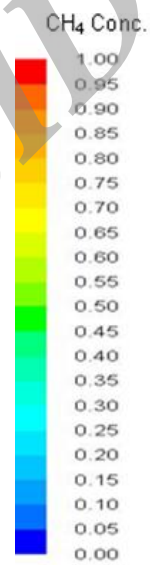

(c) Gas distribution in plane 70 m above the face.
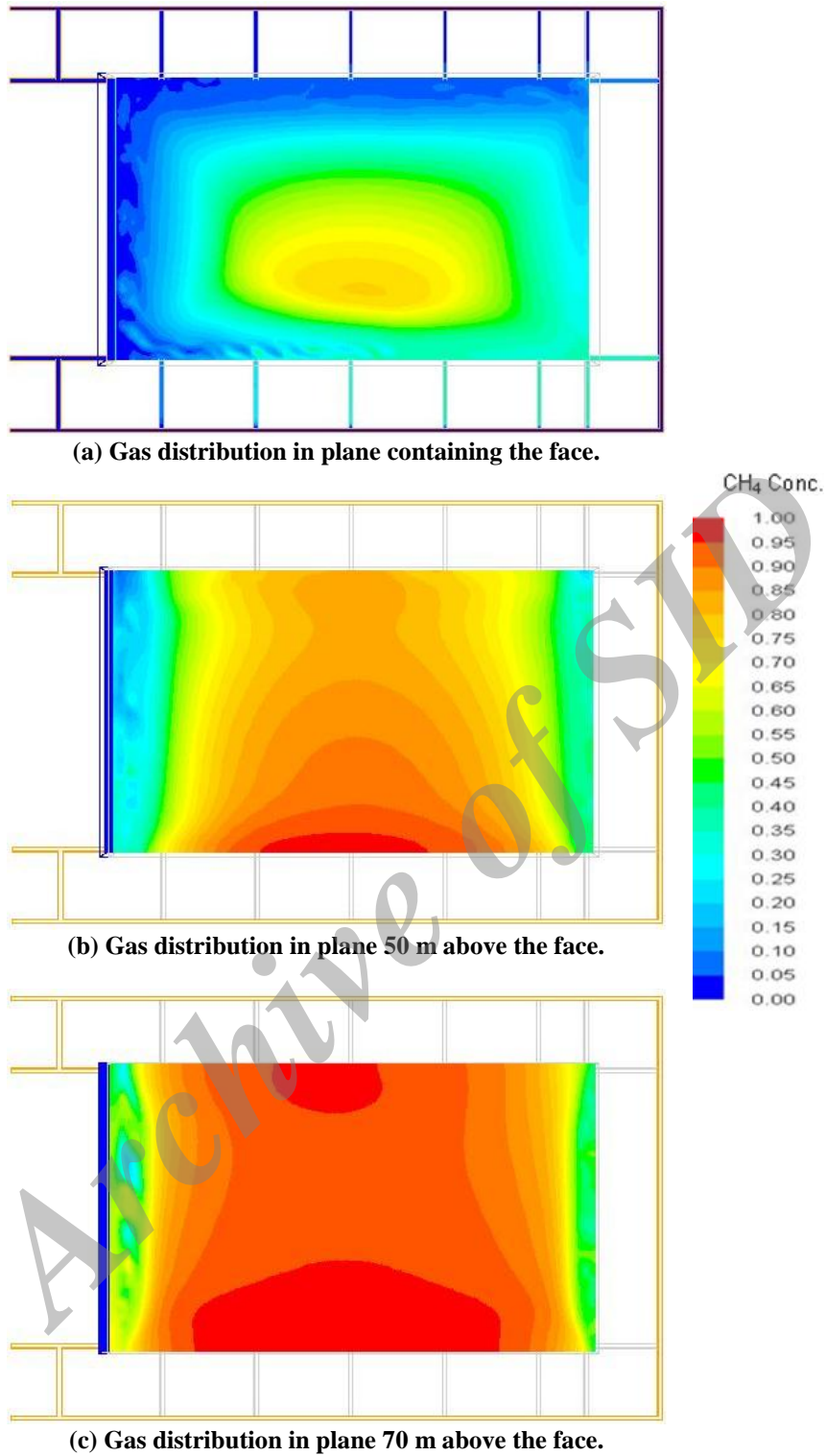
Figure 9. Goaf gas distribution for a panel with MG updip.

200

(a) Gas distribution in plane containing the face.

(b) Gas distribution in plane 50 m above the face.

CH₄ Conc.

1.00
0.95
0.90
0.85
0.80
0.75
0.70
0.65
0.60
0.55
0.50
0.45
0.40
0.35
0.30
0.25
0.20
0.15
0.10
0.05
0.00

(c) Gas distribution in plane 70 m above the face.
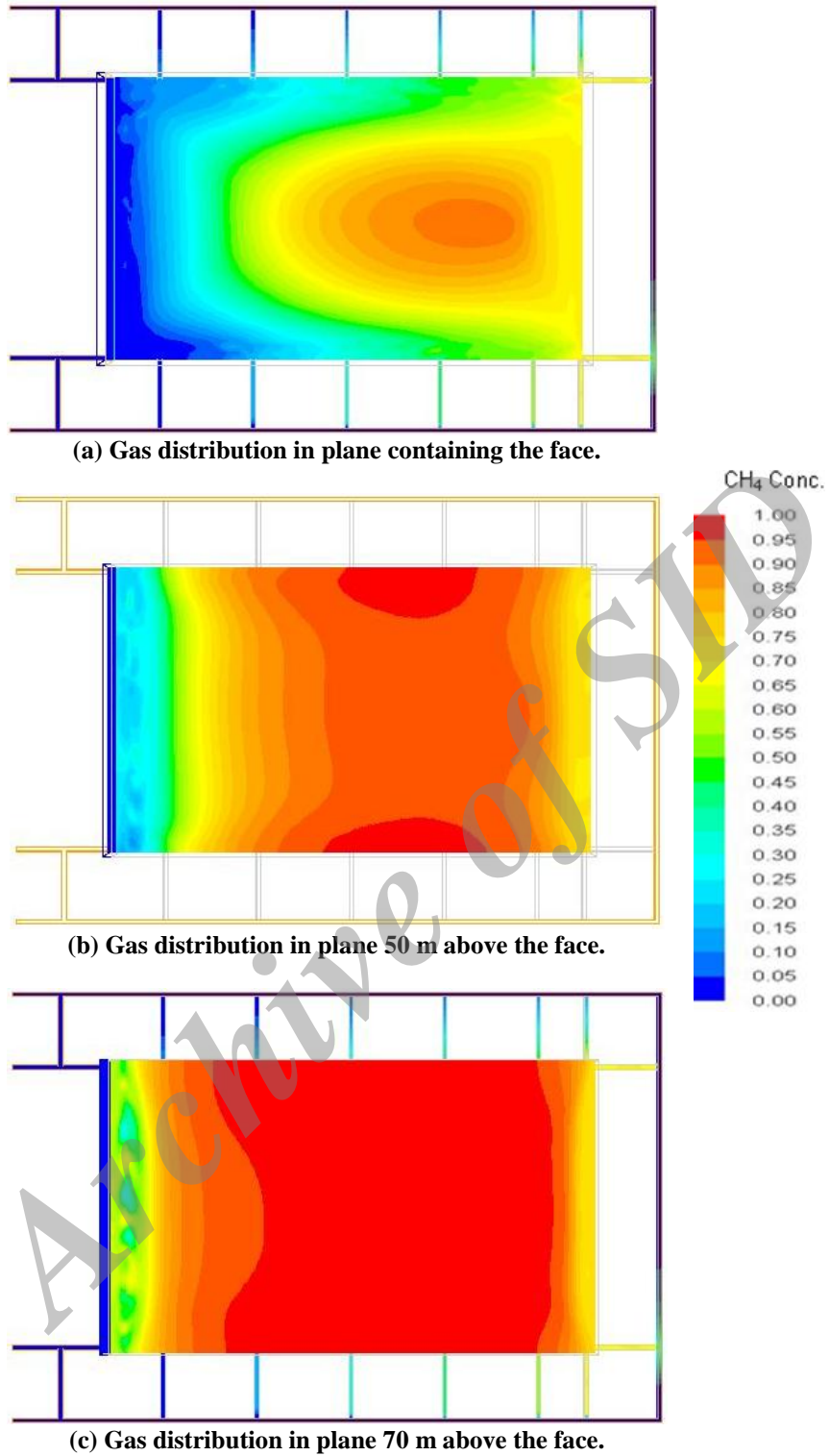
Figure 10. Goaf gas distribution for a panel with face downdip.

201

(a) Gas distribution in plane containing the face.

(b) Gas distribution in plane 50 m above the face.

(c) Gas distribution in plane 70 m above the face.

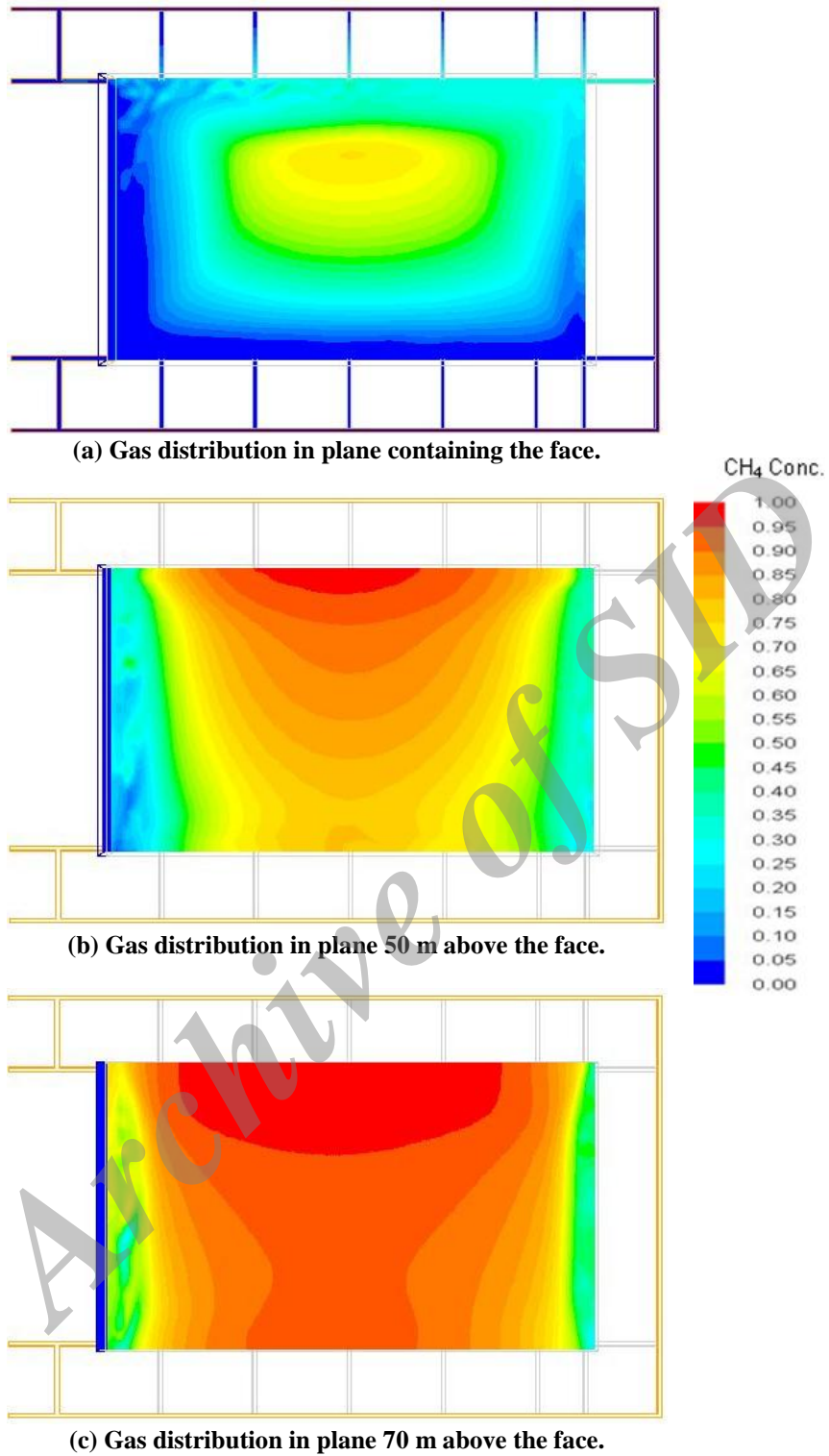**Figure 11. Goaf gas distribution for a panel with face updip.**

202
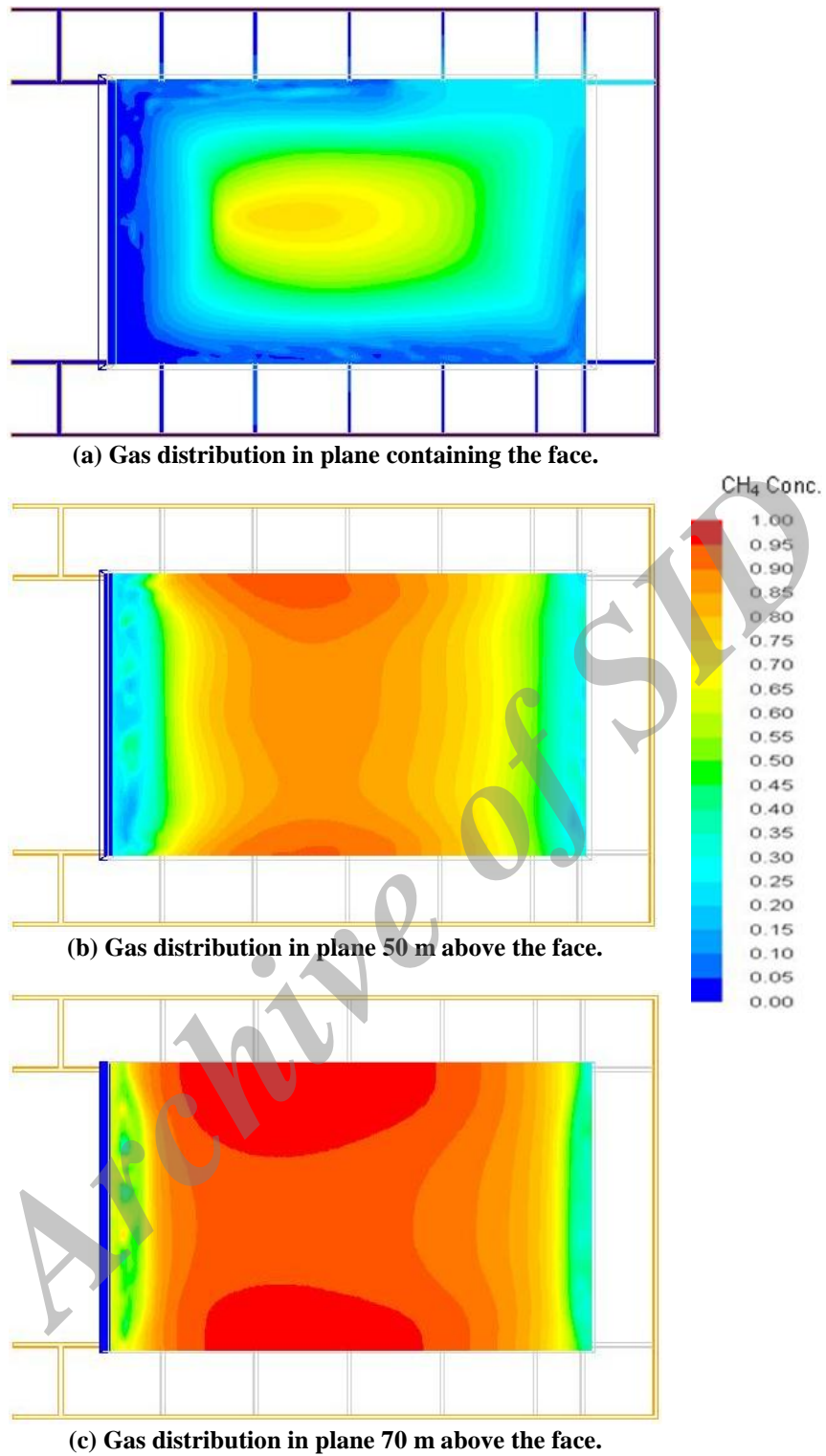
Nomenclature

$\vec{V}$	Velocity vector
$\vec{f}$	Body force vector per unit mass
$\vec{S}$	Source vector per unit mass
p	Static pressure
Y	Mass fraction of species
u_i	Velocity along i/x direction
Dm	Coefficient of mass diffusivity
Dij	Viscous resistance coefficient
Cij	Inertia resistance coefficient in porous matrix
μ	Coefficient of molecular viscosity
ρ	Mass density
$\overset{\bullet}{\omega}$	Rate of generation of mass per unit mass
τ	Stress tensor
δij	Kronecker delta
ε	Specific dissipation rate
κ	Turbulent kinetic energy
μ_T	Eddy viscosity

References

[1]. Aziz, N., Balusu, R. and Baafi, E. (1993). Application of Computational Fluid Dynamics Codes to Develop Effective Gas/Dust Control Measures in Underground Coal Mines, The Australian Coal Journal. 42: 19-27.

[2]. Balusu, R., Deguchi, G., Holland, R., Moreby, R., Xue, S., Wendtl, M. and Mallet, C. (2001). Goaf gas flow mechanics and development of gas and sponcom control strategies at a highly gassy coal mine, Australia-Japan Technology Exchange Workshop, 3-4 December, Hunter Valley, Australia, 18 P.

[3]. Balusu, R., Neil, R., Ron, P., Tim, H., Shen, Z. and Haruko, I. Optimisation of Longwall Goaf Gas Drainage & Control System, C10017, June 04.

[4]. Balusu, R., Patrick, H., Paul, H., Micheal, W. and Sheng, X. (2002). Optimum Inertisation Strategies, Proceedings of the Queensland Mining Industry Health & Safety Conference, 4-7 August, Townsville, Australia, pp. 133-144.

[5]. Balusu, R., Patric, H., Paul, H., Miceal, W. and Sheng, X. (2002). Optimum Inertisation strategies, Queensland mining industry health and safety conference.

[6]. Morla, R., Balusu, R. and Tanguturi, K. (2013). Optimum Inertisation Techniques for Blasting Gallery Method, 3rd International Workshop on Mine Hazard Prevention and Control, Brisbane, pp. 97-105.

[7]. Morla, R., Balusu, R. and Tanguturi, K. (2013). Prediction and control of spontaneous combustion in thick coal seams", Coal Operators conference, University of Wollongong., pp. 232- 239.

[8]. Morla, R., Balusu, R. and Tanguturi, K. (2014). Initiation options for BG panels and optimization using CFD modelling, The International Journal of Mining Science and Technology, IJMST-D-14-00030.

[9]. Ren, T.X., Balusu, R. and Humphries, P. (2005). Development of Innovative Goaf Inertisation Practices to Improve Coal Mine Safety, Coal Operators conference, University of Wollongong., pp. 315-322.

[10]. Tanguturi, K., Balusu, R. and Morla, R. (2014). CFD Modeling of Methane Gas Distribution and Control Strategies in a Gassy Coal Mine, The Journal of Computational Multiphase Flows.

[11]. Tanguturi, K., Balusu, R. and Morla, R. (2013). Effect of buoyancy on methane gas distribution and gas control strategies at tailgate region in a gassy coal mine", 9th International Conference on CFD in the minerals and process Industries, Melbourne, pp. 1-6.

[12]. Patnagar, V.S. (1980). Numerical Heat Transfer and Fluid Flow, Washington, DC, Hemisphere Publishing Corp.

[13]. Ansys Fluent 14.0 reference manual, 2012.

[14]. David, C.W., Turbulence modeling for CFD, DCW Industries Inc., 1994.

[15]. Roy, M., Balusu, R., Yaralagadda, S., Ting, R. and Shi, S. (2010). strategic review of gas management options for reduced GHG emissions, ACARP Project C17057.

شناخت اولیه در مورد جابجایی گاز از ناحیه تخریب‌شده در روش استخراج جبهه‌کار طولانی

K.M. Tanguturi* and R. Balusu

Energy Flagship, CSIRO, Pullenvale, Kenmore, Australia

* نویسنده مسئول مکاتبات: *krishna.tanguturi@csiro.au*

چکیده:

شناخت اولیه در مورد نحوه انتشار گاز از ناحیه تخریب‌شده معادن زغالی گازدار برای بکارگیری رویکردی موثر در گاز کشی معادن جبهه‌کار طولانی امری ضـروری است. گاز ناحیه تخریب شده که تحت نیروهای سطحی و حجمی قرار می‌گیرند براساس اینکه آیا در ناحیه سطح عمل می‌نمایند و یا برروی حجم گاز، طبقه‌بنـدی می‌شوند. از میان این نیروها، نیروهای حجمی در جابجایی گازهای ناحیه تخریب‌شده حاضر در معادن زیرزمینی بیشـتر غالبنـد. نیروهـای رانشـی ماننـد نیروهـای حجمی تقسیم می‌شوند. نیروهای رانشی عمدتاً بستگی به اختلاف چگالی در گونه‌های گازی و راستا یا هندسه پهنه دارند. اگر تغییرات دمایی قابل صـرفنظر باشد، نیروهای رانشی که عامل جابجایی گاز از ناحیه تخریب‌شده هستند، عمدتاً بستگی به راستای پهنه دارند. در این تحقیق، با بررسی عددی انجام شـده بـا اسـتفاده از روش‌های دینامیک سیالات محاسباتی (CFD)، به شناخت اولیه جابجایی گاز از ناحیه تخریب‌شده برای راستاهای مختلف پهنه پرداخته‌شده اسـت. نتـایج عـددی به‌دست‌آمده برای راستاهای مختلف پهنه نشان داد که گاز ناحیه تخریبی در زمانی که راهروی ورودی (MG) در پایین شیب قرار دارد به سمت راهـروی خروجـی (TG) حرکت می‌کند، به سمت راهروی ورودی است زمانی که راهروی ورودی در بالای شیب قرار دارد. به سمت نقطه شروع پهنه است، زمانی که جبهـه کـار در پایین شیب قرار دارد و به سمت جبهه کار است زمانی که جبهه کار در بالای شیب قرار دارد.

کلمات کلیدی: راهروی ورودی (MG)، راهروی خروجی (TG)، نقطه شروع، جبهه کار، پهنه استخراجی.